# Twisted state stability under local order parameter adaptation

Xueqin Wang, Hong He, Wende Tang, Yiju Peng, and Ya Jia [*]
*Department of Physics and Institute of Biophysics, Central China Normal University, Wuhan 430079, China*

(Received 23 July 2025; accepted 24 June 2026; published 13 July 2026)

Twisted states commonly arise in nonlocally coupled ring networks. We study the stability of twisted states in networks with higher-order interactions under the adaptive mechanism based on the local order parameter. The adaptive feedback dynamically regulates the coupling strength and thus reshapes the collective dynamics of the system. Analytical and numerical results show that higher-order adaptivity reduces the linear stability of twisted states, whereas pairwise adaptivity enhances it. Numerical simulations further demonstrate that increasing the exponent of higher-order adaptation drives the system toward more ordered states and correspondingly enlarges the basin of twisted states. Moreover, a larger coupling range reduces twisted-state stability, while in random hypergraphs, higher-order adaptivity enlarges the synchronization basin without significantly changing the linear stability. These findings reveal a nonequilibrium relationship between linear stability and basin stability and highlight the important role of adaptive regulation in higher-order network dynamics.

DOI: 10.1103/p2wd-nfbr

## I. INTRODUCTION

Stability analysis of nonlinear systems plays an important role in many complex systems. It is widely used in many fields such as power system stabilization [1,2], neuronal network activity regulation [3–5], and food chain stabilization [6,7]. Traditionally, the response of a system to small perturbations has been evaluated by linear stability analysis, the core tools of which include the Lyapunov exponent and eigenvalue spectrum [8,9]. However, when large perturbations occur, the linear stability of local concepts is not sufficient to reflect the overall stability of the system. Thus, basin stability measures global stability by estimating the probability of the system reaching the target attractor under random initial conditions [10–12]. Unlike linear stability, basin stability provides a global perspective that can reveal the robustness of the attractor and the multistability structure of the system. Linear stability and basin stability together constitute a complete framework for understanding the stability of nonlinear systems [13,14].

The importance of higher-order interactions has been significantly emphasized recently in the study of nonlinear systems. The microstructure of higher-order interactions affects burstiness as well as bistability, and determines the nature of collective behavioral transitions [15]. Simple complex forms and hypergraphs are considered as the two main mathematical frameworks when modeling higher-order interactions [16,17]. These two approaches can have opposing effects on synchronization: the former inhibits it, while the latter promotes it [18]. The deeper study of higher-order interactions helps us to understand processes such as cooperation in social networks [19], transmission pathways of infectious diseases [20], and dynamics in nervous systems [21,22]. The Kuramoto model, a standard tool for analyzing phase synchronization, is widely used to model and analyze high-dimensional coupled systems [23,24]. But many of these studies have focused on all-to-all network topologies [25,26]. In fact, higher-order interactions also exist in networks with nonlocal coupling. For example, connections between nanoelectric oscillators have been experimentally found to embody this mechanism [27]. In addition, stable attractors in more sparsely connected nonlocal coupled networks have various twisted states in addition to synchronized states [28]. The network topology [29] and link density [30] not only change the stability of the twisted state, but also affect the shape and size of the twisted state basin.

In many real-world oscillating systems (e.g., neural circuits, social systems), node connections adjust dynamically in response to the network's state [31–34]. In other words, the network is able to reshape its connection structure based on local or global activity patterns, a property known as adaptivity [35]. In neuronal networks, spike-time-dependent plasticity (STDP), which underlies learning, memory formation, and functional differentiation in the brain [36–39]. In phase oscillator systems, adaptive mechanisms usually describe the regulation of coupling strength through the global order parameter or instantaneous phase differences, thereby shaping the resulting collective dynamics [40–43]. Compared with adaptive schemes based on the global order parameter [44,45], local feedback adaptation more directly captures the influence of neighboring interactions on individual node dynamics. In particular, the local order parameter provides a natural measure of neighborhood coherence, and its modulus can therefore be used as a real-valued feedback signal to regulate the effective coupling strength. This setting offers an effective description of activity-dependent local interactions and makes it possible to examine how adaptive regulation reshapes the stability of twisted states.

In this paper we systematically explore the specific effects of coupling strength on the stability of twisted states under

[*]Contact author: jiay@ccnu.edu.cn

 

adaptive regulation. We combine numerical simulations with theoretical analyses, the latter specifically by constructing Jacobian matrices and calculating the maximum Lyapunov exponent to assess the linear stability of different twisted states. The results show that enhancing the strength of the higher-order adaption weakens the linear stability of the twisted state. However, it also drives the system to evolve from a random initial state toward a more coherent and ordered state, eventually stabilizing in twisted states. In other words, the enhancement of the higher-order adaption enlarges the basin of the twisted state. In contrast, when an adaptive regulation mechanism is introduced in pairwise interactions, we observe the opposite trend: the enhancement of pairwise adaptivity enhances the linear stability of the twisted state under certain conditions, but shrinks its basin accordingly.

The structure of this paper is organized as follows: In Sec. II we introduce a higher-order ring network model with adaptive mechanisms and provide a theoretical analysis of the linear stability of the twisted state, along with the statistical measures used. In Sec. III we discuss the linear stability and basin stability of the twisted state from both numerical simulations and theoretical analysis. Finally, we draw our conclusions in the last section.

## II. MODEL

Consider an oscillatory system with adaptive nonlocal coupling, in which case the phase dynamics of a single oscillator follows the following equation:

$$\begin{aligned}\dot{\theta}_i =& \frac{k_1|O_i|^\alpha}{2r}\sum_{j=i-r}^{i+r}\sin(\theta_j-\theta_i)\\ &+\frac{k_2|O_i|^\beta}{2r(2r-1)}\sum_{j=i-r}^{i+r}\sum_{k=i-r}^{i+r}\sin(\theta_j+\theta_k-2\theta_i),\end{aligned} \tag{1}$$

where the local order parameter $O_j = \frac{1}{2r+1}\sum_{k=j-r}^{j+r} e^{\mathrm{i}\theta_k}$. $k_1$ and $k_2$ are the coupling strengths of the 1-hyperedge and 2-hyperedge forms, respectively. The parameters $\alpha$, $\beta$ describe the adaptive properties of the system. Specifically, as the degree of feedback from the surrounding oscillators to the ith oscillator through pairwise and higher-order interactions. The range of coupling is denoted by $r$, with $r = 2$ unless stated otherwise. In addition, the eigenfrequency of all the oscillators in the model is set to be the same. Since the system has global phase rotational symmetry, we can simplify the dynamics analysis by normalizing this common frequency to 0 in the rotational coordinate system.

The twisted state is described by $\theta_i = 2\pi iq/N + C$, where $q$ denotes the number of twisted turns [46]. Substituting this into Eq. (1) results in $\Delta\dot{\theta}_i = 0$, indicating that twisted state is an equilibrium point. Next, we analyze the linear stability of the twisted state by finding the maximum eigenvalue theory of the Jacobian matrix. The elementary form of the Jacobian matrix for any equilibrium point is as follows:

$$\begin{aligned}J_{ij} =& \frac{k_1|O_i|^\alpha}{2r}A_{ij}\cos(\theta_j^*-\theta_i^*)\\ &+\frac{k_2|O_i|^\beta}{2r(2r-1)}\sum_{k=1}^{n}B_{ijk}\cos(\theta_j^*+\theta_k^*-2\theta_i^*),\\ J_{ii} =& -\sum_{\substack{j=1\\ j\neq i}}^{n}J_{ij},\end{aligned} \tag{2}$$

where $A_{ij}$ denotes the adjacency matrix for pairwise interactions, and $B_{ijk}$ denotes the tensor for three-body interactions. Specifically, $A_{ij} = 1$ when node $j$ is within the range $r$ of node $i$, and $A_{ij} = 0$ otherwise; $B_{ijk} = 1$ when both $j$ and $k$ are within the range $r$ of node $i$, and $B_{ijk} = 0$ otherwise. It follows from the rotational symmetry of the topology and the linear phase difference of the twisted states that this Jacobian matrix is a cyclic symmetric matrix, then the matrix is

$$\boldsymbol{J} = \begin{bmatrix} J_0 & J_1 & \cdots & J_2 & J_1\\ J_1 & J_0 & J_1 & \cdots & J_2\\ \vdots & J_1 & J_0 & \ddots & \vdots\\ J_2 & \vdots & \ddots & \ddots & J_1\\ J_1 & J_2 & \cdots & J_1 & J_0\end{bmatrix}. \tag{3}$$

Next, we will be concerned with the derivation of the local order parameter. According to the definition of twisted state and assume that the phase difference between neighboring oscillators is $\delta = \frac{2\pi q}{N}$. Substituting the above assumptions into the definition of the local order parameter yields

$$\begin{aligned}O_j &= \frac{1}{2r+1}\sum_{n=-r}^{r} e^{\mathrm{i}[\delta(j+n)+C]}\\ &= \frac{e^{\mathrm{i}(\delta j+C)}}{2r+1}\sum_{n=-r}^{r} e^{\mathrm{i}\delta n}.\end{aligned} \tag{4}$$

According to the symmetry of the summation,

$$\sum_{n=-r}^{r} e^{\mathrm{i}\delta n} = e^{-\mathrm{i}r\delta}\sum_{n=0}^{2r} e^{\mathrm{i}\delta n} = \frac{\sin[(r+\frac{1}{2})\delta]}{\sin(\frac{\delta}{2})}, \tag{5}$$

so the local order parameter can be written as

$$O_j = \frac{e^{\mathrm{i}(\delta j+C)}}{2r+1}\frac{\sin[(r+\frac{1}{2})\delta]}{\sin(\frac{\delta}{2})}. \tag{6}$$

Further, the modulus of the local order parameter is

$$|O_j| = \frac{1}{2r+1}\left|\frac{\sin[(r+\frac{1}{2})\delta]}{\sin(\frac{\delta}{2})}\right|. \tag{7}$$

Thus, for a fixed number of nodes and coupling range, the local order parameter of the twisted state depends only on the number of twisted turns and is not directly related to the specific nodal phase. We know that the eigenvalues of a cyclic matrix are the discrete Fourier transforms of the elements of the first row, so the $k$th eigenvalue of the cyclic matrix (3) is

$$\lambda_p(\boldsymbol{J}) = \sum_{s=0}^{N-1} J_s e^{2\pi\mathrm{i}ps/n}, \quad 0 \leqslant p \leqslant N-1, \tag{8}$$

where $J_s = J_{N-s}$ for $\lfloor N/2 \rfloor < s < N$, and thus all eigenvalues $\lambda_p$ of the matrix are real numbers. The relationship between $J_s$ and the elements of the Jacobian matrix is given by $J_s = J_{1,s+1}$. In the translational direction (i.e., the direction in which all the oscillators change at the same time), the relative phase difference between the oscillators remains constant. As a result, the system is insensitive to perturbations in this direction and the corresponding eigenvalue is zero, i.e., $\lambda_0 = 0$. For the twisted state with the coupling range $r = 2$ and the number of twisting turns $q$, the combined analysis above yields the expression of $J_s(0 < s \leqslant r)$ as follows:

$$\begin{aligned} J_1 &= \frac{k_1}{4}\left|\frac{\sin\left(\frac{5\pi q}{N}\right)}{5\sin\left(\frac{\pi q}{N}\right)}\right|^{\alpha}\cos\left(\frac{2\pi q}{N}\right) + \frac{k_2}{6}\left|\frac{\sin\left(\frac{5\pi q}{N}\right)}{5\sin\left(\frac{\pi q}{N}\right)}\right|^{\beta} \\ &\quad\times\left[1+\cos\left(\frac{2\pi q}{N}\right)+\cos\left(\frac{6\pi q}{N}\right)\right], \\ J_2 &= \frac{k_1}{4}\left|\frac{\sin\left(\frac{5\pi q}{N}\right)}{5\sin\left(\frac{\pi q}{N}\right)}\right|^{\alpha}\cos\left(\frac{4\pi q}{N}\right) + \frac{k_2}{6}\left|\frac{\sin\left(\frac{5\pi q}{N}\right)}{5\sin\left(\frac{\pi q}{N}\right)}\right|^{\beta} \\ &\quad\times\left[1+\cos\left(\frac{2\pi q}{N}\right)+\cos\left(\frac{6\pi q}{N}\right)\right], \\ J_0 &= -2\sum_{s=1}^{r} J_s. \end{aligned} \tag{9}$$

Bringing the above equation into Eq. (8) yields all the eigenvalues of the twisted state for a twisted number of turns $q$. The maximum Lyapunov exponent in the direction of the small perturbation that deviates from the synchronized flow pattern is $\lambda_{\max} = \max\{\lambda_1, \lambda_2, \ldots, \lambda_{n-1}\}$. If $\lambda_{\max} < 0$, it means that the $q$-twisted state is linearly stable.

In nonlocal coupled networks with higher-order interactions, the system evolves and stabilizes to different steady states. In order to quantitatively portray the difference in coherence of these steady states, we introduce the strength of incoherence (SI) [47]:

$$\mathrm{SI} = 1 - \frac{\sum_{i=1}^{N} S_i}{N},\ s_i = \Theta(\varepsilon - \sigma_i), \tag{10}$$

where $\Theta$ is the Heaviside function, $\varepsilon$ a very small predefined threshold, and $\sigma_i$ denotes the local phase standard deviation of the $i$th oscillator:

$$\sigma_i(t) = \sqrt{\frac{1}{2r}\sum_{m=i-r}^{i+r}[\Delta\theta_m(t) - \langle\Delta\theta(t)\rangle]^2}. \tag{11}$$

Here $\Delta\theta_m(t)$ is the phase difference between neighboring oscillators at moment $t$, and $\langle\Delta\theta(t)\rangle$ is the average value of $\Delta\theta_m(t)$ in the interval $[i-r, i+r]$ in the neighborhood of oscillator $i$. If the phase difference between an oscillator $i$ and its neighboring oscillators is highly consistent ($\sigma_i < \varepsilon$), then $s_i = 1$. This indicates that the local region is in a synchronous state. Conversely, if $\sigma_i > \varepsilon$, $s_i = 0$, which indicates that there are significant phase fluctuations in the region, and it is in a nonsynchronous state. By the above definition, the range of values of SI is limited to be between 0 and 1. SI = 0 and SI = 1 denote coherent and incoherent states, respectively. Both the synchronized state and twisted state correspond to SI = 0, indicating coherence. Values of 0 < SI < 1 denote the chimeric state.

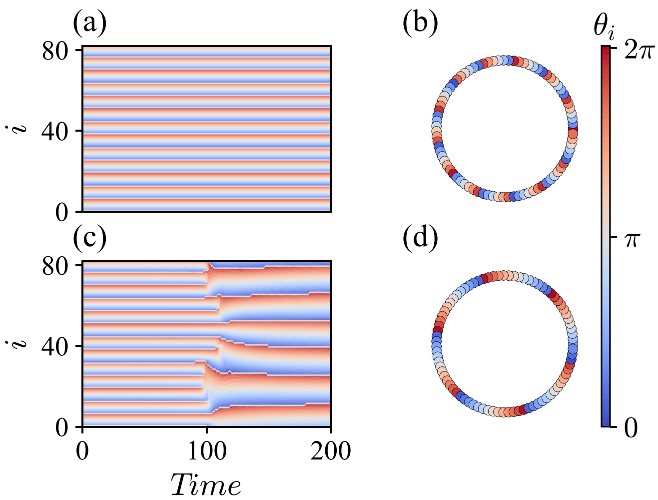


FIG. 1. Evolution of phase over time in a network of nonlocally coupled oscillators without considering higher-order adaption (a) $\beta = 0$ and with higher-order adaption considered (c) $\beta = 1$. Panels (b) and (d) are the ring phase distributions at the end moments of (a) and (c), respectively. The other parameters are $k_2 = 1$ and $q = 13$. When higher-order adaption is introduced, the twisted state of $q = 13$ loses linear stability. The oscillator network phase evolves with time and eventually stabilizes to the twisted state of $q = 6$.

## III. RESULTS

### A. Linear stability of twisted states

We set the pairwise coupling strength $k_1 = 1$ without loss of generality, as it can be absorbed into a rescaled time variable. This simplification does not affect the qualitative behavior of the system. Based on this setup, we focus on exploring the effect of the higher-order adaptivity parameter $\beta$ on the stability of the system.

In order to investigate the linear stability of the twisted state, we combine numerical simulations with theoretical analysis for verification against each other. Figure 1 presents numerical simulation results illustrating the impact of higher-order adaptation on the evolution of the $q = 13$ twisted state. The initial phase of the network is configured to apply a small perturbation on the $q = 13$ twisted state basis. In particular, Figs. 1(a) and 1(c) correspond to the phase spatiotemporal plots without ($\beta = 0$) and with ($\beta = 1$) higher-order adaptation, respectively. The spatial distributions of the phase at the corresponding final moment $t = 200$ in the ring network are shown in Figs. 1(b) and 1(d). As can be seen, in the case of $\beta = 0$ [Figs. 1(a) and 1(b)], the system always maintains the initial $q = 13$ twisted state. The phase distribution remains basically unchanged over time, which indicates that the state is linearly stable. On the contrary, when higher-order adaptive ($\beta = 1$) is considered, it can be observed from Fig. 1(c) that the system undergoes a state transition at about $t = 100$. The phase distribution gradually departs from the twisted distribution of $q = 13$, and finally stabilizes to a $q = 6$ twisted state, as shown in Fig. 1(d). This indicates that the originally

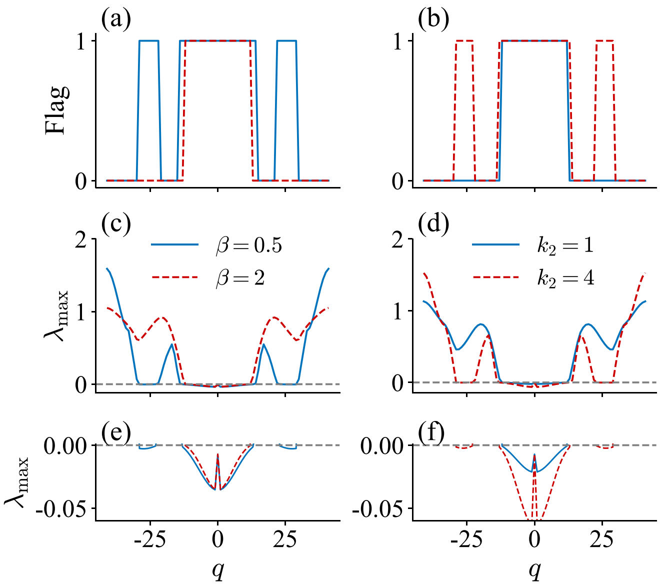


FIG. 2. The left and right columns show the linear stability results of the twisted state under different higher-order adaptive strengths and different higher-order coupling strengths, respectively. Panels (a) and (b) show the numerical simulation results, where Flag = 1 indicates that the corresponding $q$-twisted state is linearly stable, and Flag = 0 indicates that its linear stability is lost; (c) and (d) show the maximum Lyapunov exponent $\lambda_{\max}$ obtained from the theoretical analysis, and the corresponding twisted state is linear if $\lambda_{\max} < 0$; (e) and (f) are enlarged plots of the region $\lambda_{\max} < 0$ in (c) and (d), respectively, to show the stabilization interval more clearly. The parameters are set as follows: $k_2 = 1$ in (a), (c), and (e); $\beta = 1$ in (b), (d), and (f).

stabilized $q = 13$ twisted state loses its linear stability after the introduction of the higher-order adaptive mechanism.

Further, we investigate the effect of the variation of the higher-order adaptive strength on the linear stability of the twisted states of each order. Figure 2 shows the stability of each twisted state under two combinations of higher-order adaptivity $\beta$ and coupling strength $k_2$, where Figs. 2(a) and 2(b) show the numerical simulation results under the corresponding conditions. The parameter Flag is set to 1 or 0 to indicate whether the twisted state is linearly stable or unstable, respectively. In other words, Flag determines whether the system maintains the phase distribution of the initial $q$-twisted state during the evolution. We analyze the numerical simulation of a total of 83 different twisted states for all $q \in [0, 82]$ in a nonlocally coupled ring network with an oscillator number of $N = 83$. Since the phase distribution of the twisted states is the same for $q$ and $N - q$, the equivalent interval of $q \in [-41, 41]$ is used in the figure to represent the twisted states. As seen in the figure, the stability is symmetric with respect to $q = 0$, indicating that the $q$-twisted state has the same linear stability as the $-q$-twisted state.

Under the smeller higher-order adaptive parameter ($\beta = 0.5$), the twisted states with linear stability (Flag = 1) are distributed in three discontinuous intervals: $-29 \leqslant q \leqslant -22$, $-14 \leqslant q \leqslant 14$, and $22 \leqslant q \leqslant 29$. When the higher-order adaptive parameter is increased to $\beta = 2$, only the twisted states in the range of $-12 \leqslant q \leqslant 12$ remain stable, as shown in Fig. 2(a). In summary, the increase of higher-order adaptivity significantly shrinks the range of linearly stabilized twisted states, resulting in more twisted states being destabilized.

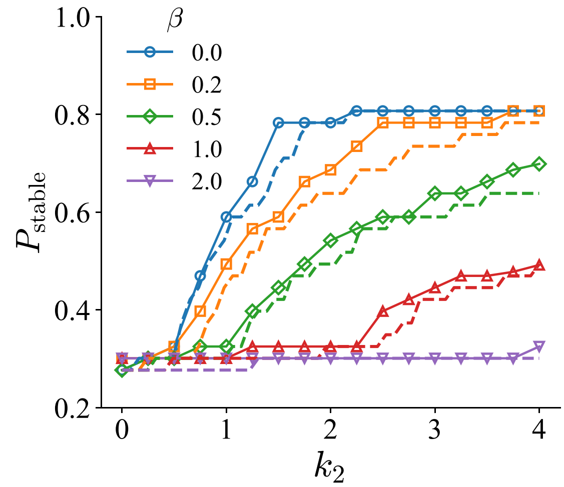


FIG. 3. Variation of the proportion of stabilized twisted states with higher-order coupling strength $k_2$ for different higher-order adaptive parameters. The dotted line indicates the numerical simulation results, and the dashed line indicates the theoretical calculation results. As $k_2$ increases, more twisted states become linearly stable, while increasing $\beta$ suppresses the stability of twisted states. Stronger higher-order adaptivity reduces the stabilizing influence of $k_2$ on twisted states.

Figure 2(b) shows the linear stability performance of each twisted state in the presence of higher-order adaptivity ($\beta = 1$) for different higher-order coupling strengths ($k_2 = 1$ and $k_2 = 4$). When $k_2 = 1$, the range of stabilized twisted states is $-12 \leqslant q \leqslant 12$. While the range of stabilized twisted states is significantly enlarged when $k_2$ is increased to 4, including $-29 \leqslant q \leqslant -23$, $-13 \leqslant q \leqslant 13$, and $23 \leqslant q \leqslant 29$. It can be seen that increasing the higher-order coupling strength leads to more twisted states obtaining the linear stability under consideration of the higher-order adaptive. Figures 2(c) and 2(d) give the results of theoretical analysis, showing the maximum Lyapunov exponent $\lambda_{\max}$ with respect to the number of torsional turns $q$. Figures 2(e) and 2(f) show the enlarged plots of the region of $\lambda_{\max} < 0$ in Figs. 2(c) and 2(d), respectively. The stable twisted state range ($\lambda_{\max} < 0$) in the theoretical analysis closely matches the Flag = 1 region from the numerical simulations. This shows that there is a better correspondence between our theoretical analysis and the numerical simulation.

We comprehensively investigate how higher-order adaptive parameter affects twisted state stability. Specifically, we calculate the relationship between the proportion of stable twisted state $P_{\text{stable}}$ and the higher-order coupling strength $k_2$. These calculations are performed through numerical simulations and theoretical analysis across different values of the adaptive parameter $\beta$. As shown in Fig. 3, the dotted line indicates the numerical simulation results and the dashed line indicates the theoretical calculation results. For the reference case without adaptation ($\beta = 0$), as $k_2$ gradually increases from 0, $P_{\text{stable}}$ rapidly increases from about 0.3 and finally stabilizes at about 0.8. As the higher-order adaptive parameter $\beta$ increases, the rise becomes smoother and stabilizes at a lower value. When $\beta$ reaches 2.0, $P_{\text{stable}}$ almost no longer changes with the change of $k_2$, indicating that higher-order coupling's stabilizing effect is greatly reduced. In addition, for the same higher-order coupling strength, $P_{\text{stable}}$ decreases continuously with the increase of $\beta$. This further indicates that the higher-order adaptivity suppresses the linear stability of the twisted state in general. At the same time, our results also show that enhancing the higher-order coupling strength still contributes to the stability of the system under the consideration of higher-order adaptivity, a trend consistent with the previous findings [47].

The theoretical values of the stabilized twisted state proportion $P_{\text{stable}}$ in Fig. 3 are generally lower than the numerical simulation results. This discrepancy essentially reflects the difference between finite timescale effects and theoretical asymptotic analysis. Specifically, for a given coupling strength and adaptive strength, some twisted states theoretically yield $\lambda_{\max}$ slightly larger than zero. However, within our finite simulation window ($T = 200$), no observable phase evolution occurs in numerical simulations. This leads to a higher proportion of stable states in simulations compared to theoretical predictions. It is also worth noting that the increase in higher-order adaptive parameter is physically equivalent to weakening the higher-order interactions between the oscillators. For a twisted state with a deterministic initial phase, its corresponding local adaptive parameters are deterministic. When $\beta$ increases, the actual influence of the higher-order coupling terms on the evolution of the system becomes smaller. The system is more inclined to gradually evolve into a stable state with a smaller number of twisted turns, thus reducing the linear stability of the twisted state. Therefore, increased higher-order adaptive strength undermines the system's ability to maintain complex structural stability, suppressing twisted state linear stability as a whole.

### B. Basin stability in twisted states

Basin stability refers to the probability distribution of the final evolution of the system to the individual attractors after starting from different stochastic initial conditions [11–13]. The resulting distribution reflects the robustness of the attractors to initial perturbations. Basin size is then a specific measure of this robustness.

For a system with $N = 83$ units, the phase space is the high-dimensional torus $[0, 2\pi)^{83}$. In such a high-dimensional setting, an exhaustive sampling of all attractor basins is not feasible. Therefore, the basin size considered here are estimated by a Monte Carlo sampling over random initial phase configurations. Accordingly, the relevant criterion is the convergence of the estimated statistical quantities with respect to the number of sampled initial conditions, rather than an exhaustive discretization of the full phase space. Figure 4(a) first justifies the choice of the number of random initial conditions used in the statistical analysis. At $\beta = 0$, the mean incoherent intensity SI of the stable state increases with increasing higher-order coupling strength $k_2$. The results obtained with different numbers of random initial conditions $N_{\text{reps}}$ indicate that the curves for $N_{\text{reps}} = 5000$ and 10 000 are nearly

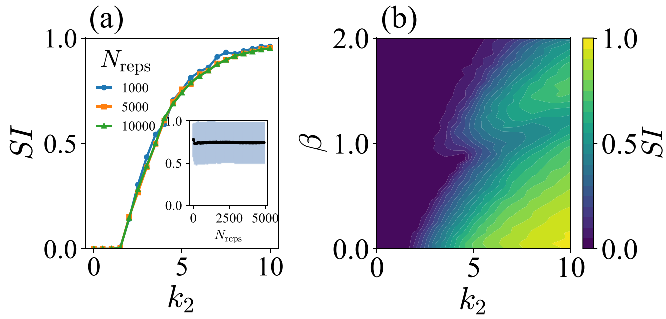


FIG. 4. (a) Dependence of the mean incoherent intensity SI of the stable state on the higher-order coupling strength $k_2$ for different numbers of random initial conditions at $\beta = 0$. The inset shows the mean incoherent intensity and its error as functions of the number of random initial conditions $N_{\text{reps}}$ for $k_2 = 5$. (b) Distribution of the incoherent intensity SI in the plane of $(k_2, \beta)$ parameters. Each set of data under the $(k_2, \beta)$ parameters is based on the simulation results at running time $t = 800$ and statistically obtained from 5000 sets of random initial conditions. The results show that the degree of incoherence of the attractor state of the system decreases with the increase of $\beta$, while increasing $k_2$ enhances the incoherence of the system.

indistinguishable, whereas the curve for $N_{\text{reps}} = 1000$ shows only slight deviations in the large-$k_2$ region. Moreover, the inset, plotted for $k_2 = 5$, shows that both the mean value of SI and its error become essentially unchanged when $N_{\text{reps}} > 2500$. Therefore, in the following analysis of the $(k_2, \beta)$ parameter plane, we adopt $N_{\text{reps}} = 5000$ random initial conditions for each parameter pair, which provides a reasonable compromise between statistical accuracy, smoothness of the results, and computational cost.

As shown in Fig. 4(b), for $k_2 < 2$, the system eventually tends to a coherent state, regardless of the value of the higher-order adaptive strength $\beta$. When $k_2 > 2$, the noncoherence gradually decreases with $\beta$, indicating that the higher-order adaptation helps to enhance the ability of the system to converge to the ordered state. On the contrary, the increase of $k_2$ significantly increases the degree of incoherence of the system, leading to a more complex and diverse structure of the attractor state. As the exponent of adaptivity increases, the coherence of the attractor increases, so what kind of transition does the attractor undergo in the process? In order to explore the different states of the system from incoherent to coherent dynamics, we discuss the example of the $k_2 = 5.0$. Figure 5(a) shows the variation of the proportion of ordered states with $\beta$. In this paper we adopt $|O_i| > 0.85$ as an empirical threshold for determining the locally ordered state, which ensures that $P_{\text{order}} = 1$ when $\beta$ is sufficiently large. $P_{\text{order}}$ calculates the proportion of oscillators in the oscillator network that satisfy the $|O_i| > 0.85$ condition, and is used to measure the degree of orderliness of the system [47]. $P_{\text{order}} = 0$ and $P_{\text{order}} = 1$ denote the disordered state and the ordered state (twisted state), respectively, and $0 < P_{\text{order}} < 1$ indicates the chimeric state.

The results show that $P_{\text{order}}$ increases monotonically with the exponent of higher-order adaptation and then reaches a stable value. This indicates that increasing the exponent of higher-order adaptation helps the system to transition from a disordered to an ordered state. Further, Figs. 5(b)–5(e) show

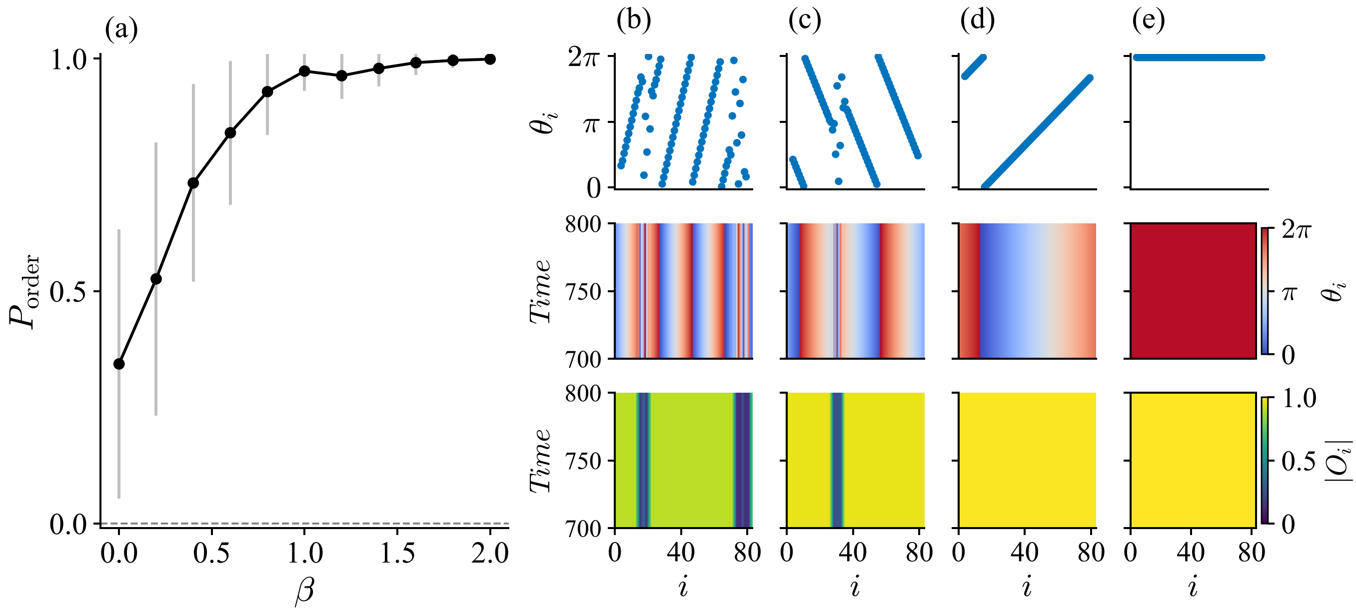


FIG. 5. The increase of higher-order adaptive parameter drives the system to gradually transition from a disordered state to an ordered state. (a) The proportion of the final evolution to the ordered state as a function of $\beta$ for $10^4$ simulations. The right panels (b)–(e) correspond to the four scenarios of $\beta = 0$, 0.5, 1.0, and 2.0, respectively. In each group: the upper panel shows the phase distribution of the system at the last moment; the middle and lower panels show the spatiotemporal patterns of the phase evolution and the local order coefficients during the last 100 s, respectively. The higher-order coupling strength is fixed at $k_2 = 5.0$.

the phase distribution at the end moment, the phase spatiotemporal patterns, and the spatial-temporal map of the $|O_i|$ for different $\beta$ values. As shown in Fig. 5(b), when $\beta = 0$, the system ends up in the chimeric state. In this state, a small portion of the oscillators are in the ordered state ($|O_i| = 1$), while most remain asynchronous with chaotic phases. At $\beta = 0.5$ and $\beta = 1.0$ [Figs. 5(c)–5(d)], the system eventually stabilizes to a stable twisted state with the number of twisted turns $q = 1$. When $\beta = 2$ [Fig. 5(e)], the synchronized state becomes the only attractor. In conclusion, as $\beta$ increases, the system gradually transitions from a completely disordered state to a stable linear phase-aligned state. Meanwhile, the local order parameter $|O_i|$ is comprehensively enhanced, indicating an overall increase in the synchronization level of the system. This result emphasizes the important role of the introduction of structural adaptive mechanisms in higher-order coupling in regulating the emergence of ordered behavior.

The above results show that higher-order adaption reduces the linear stability of the twisted state, but makes the ordered state more likely to appear. Next, we further explore the change of higher-order adaptation on the attractor basin during the process of the system going from a disordered to an ordered state. Figure 6 shows the stochastic two-dimensional slices centered on the twisted state of $q = 13$ (left column). The right column presents the corresponding occurrence probabilities of the individual twisted states for different parameters of higher-order adaptation. The cyan color in the figure indicates the twisted state with $q = 13$ and the black color indicates the nontwisted state. The slices consist of $\theta_0 + \alpha_1 P_1 + \alpha_2 P_2$, $\alpha_i \in (-\pi, \pi]$, where $P_1$ and $P_2$ are $n$-dimensional binary direction vectors and the randomly chosen $n/2$ component is set to be 1 and the rest to be 0. As shown in Fig. 6(a), when $\beta = 0.2$, the twisted state with center $q = 13$ occupies a larger area, but the basin of the nontwisted state dominates. That is, the twisted state with $q = 13$ is stable at this point, but most of the stochastic initial conditions eventually stabilize to the disordered state. In Figs. 6(b) and 6(c), when $\beta$ increases to 0.5 and 0.8, respectively, it can be seen that the areas of cyan and black regions become smaller and the other colored regions become larger. The results show that the basin of the twisted state is increasing, the stability of $q = 13$ is decreasing, and the basin of the nontwisted state is gradually decreasing. As shown in Fig. 6(d), for $\beta = 2.0$, the nontwisted state attractor vanishes, the twisted state at $q = 13$ is unstable, and the attractor is dominated by the synchronized state. This is further evidence that the enhancement of higher-order adaptivity reduces the linear stability of the twisted state. At the same time, it expands the basin size of the twisted state, allowing more random initial conditions to stabilize to the ordered twisted state.

To more comprehensively explore the effects of higher-order adaptation and higher-order coupling strength on the basin of the twisted state, we analyze the results shown in Fig. 7. The figure illustrates how the relative basin size of the twisted state varies with the higher-order coupling strength $k_2$ for three different levels of higher-order adaptation. We estimate relative basin sizes by simulating $1 \times 10^4$ random initial conditions and calculating each twisted state's stabilization probability. For smaller degrees of higher-order adaptivity [Figs. 7(a) and 7(b)], when $k_2 < 2$, the system attractors are all twisted states. Among them, twisted states with a smaller number of turns have larger basins, with the synchronized state having the largest basin. As $k_2$ increases, the basins of the twisted states with small number of turns gradually decrease. On the contrary, the basins of the twisted states with larger number of turns gradually increase. With further increase in

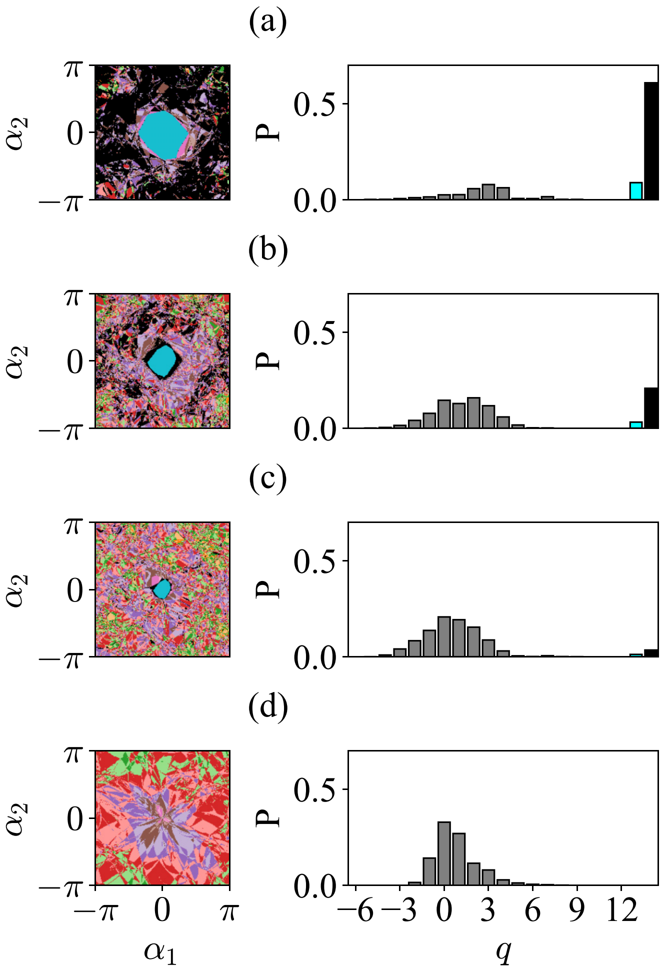


FIG. 6. Centered on the twisted state of $q = 13$, the left panels show the variation of the attraction domains in the two-dimensional slice, and the right panels show the corresponding probability of occurrence of each twisted state. Results are shown for (a) $\beta = 0.2$, (b) $\beta = 0.5$, (c) $\beta = 0.8$, and (d) $\beta = 2.0$. The black area indicates the attraction domains of all non-twisted states. The cyan area corresponds to the twisted state with $q = 13$, and the other colors indicate the twisted states with different numbers of turns, respectively. The results show that the linear stability of the $q = 13$ twisted state decreases with increasing $\beta$, whereas its attraction domain expands, indicating stronger basin stability.

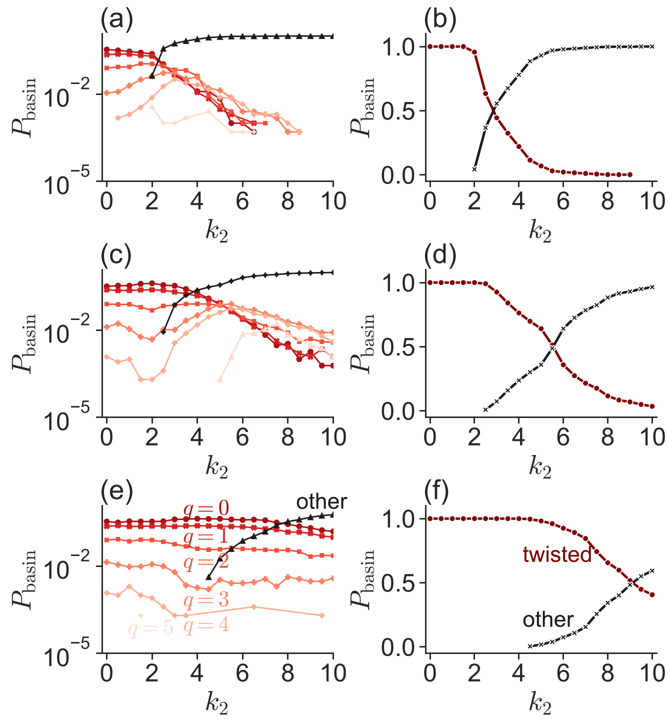


FIG. 7. Variation of the attraction basin size with the higher-order coupling strength $k_2$ for different adaptive strengths (a), (b) $\beta = 0.2$, (c), (d) $\beta = 1.0$, and (e), (f) $\beta = 2.0$. The left column shows the basin sizes of different twisted states, and the right column shows the total basin sizes of the twisted and other states. The increase of the $\beta$ slows the decrease of the basin of the twisted state with increasing $k_2$, suggesting that higher-order adaption helps maintain the stability of the twisted state basin to some extent.

$k_2$, all the basins of each twisted state gradually decrease, and the basin of nontwisted state dominates. Figure 7(b) summarizes Fig. 7(a), where the basin of twisted state is the sum of the basins of twisted state for all the twisted turns. The results show that when $k_2 < 2.8$, the twisted state basins are larger than the nontwisted state basins, and the system is more likely to evolve to the twisted state. When $k_2 > 2.8$, the nontwisted state basins are larger than the twisted state basins, indicating that the system is more likely to fall into a disordered state.

In the case of $\beta = 1.0$ [Figs. 7(c) and 7(d)], the higher-order coupling strength corresponding to the emergence of a nontwisted state basin is higher ($k_2 = 2.5$) compared to $\beta = 0.2$. From Fig. 7(d), it can be seen that the twisted state basin decreases more slowly with increasing $k_2$, suggesting that the enhancement of the adaptive strength improves the robustness of the twisted state attractor. When $\beta = 2.0$ [Fig. 7(e)], the change in the size of individual twisted state basins with $k_2$ is not significant. Thus, an increase in the exponent of higher-order adaptivity delays the disappearance of the twisted state basins and hinders the emergence of nontwisted state basins. As a result, more stochastic initial conditions eventually evolve into ordered states. This finding further supports the earlier result that linear stability and basin stability of twisted states may exhibit opposite trends [14]. It highlights a complex trade-off between local stability and global attractiveness in the system.

Basin stability in the twisted state is enhanced after the introduction of higher-order adaptive mechanisms. The underlying mechanism of this phenomenon is that higher-order adaptation modulates the effective strength of higher-order interactions. Specifically, the effective strength of higher-order interactions is weakened when the adaptive parameter $\beta$ is increased. It has already been shown that enhanced higher-order interactions significantly weaken the basin stability of the twisted state [48]. Therefore, when higher-order adaptation is enhanced and higher-order coupling is suppressed, the system is more likely to remain near the attractor of the twisted state. This, in turn, leads to an increase in basin stability.

Correspondingly, we further speculate that if an adaptive modulation mechanism is introduced into pairwise interactions, a similar effect may occur. Specifically, as the degree of pairwise adaptation increases, the effective coupling strength

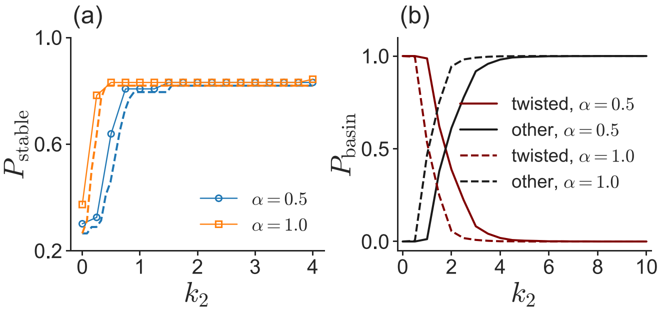


FIG. 8. (a) Variation of the proportion of stabilized twisted states $P_{\mathrm{stable}}$ with the higher-order coupling strength $k_2$ for two different pairwise adaptive strengths ($\alpha = 0.5$ and $\alpha = 1.0$). (b) The trend of the basin sizes of the twisted state and the nontwisted state with $k_2$ for different pairwise adaptive strengths. The other parameters are fixed at $\beta = 0.2$. An increase in the pairwise adaptive strength helps to improve the linear stability of the twisted state, but simultaneously decreases its basin stability.

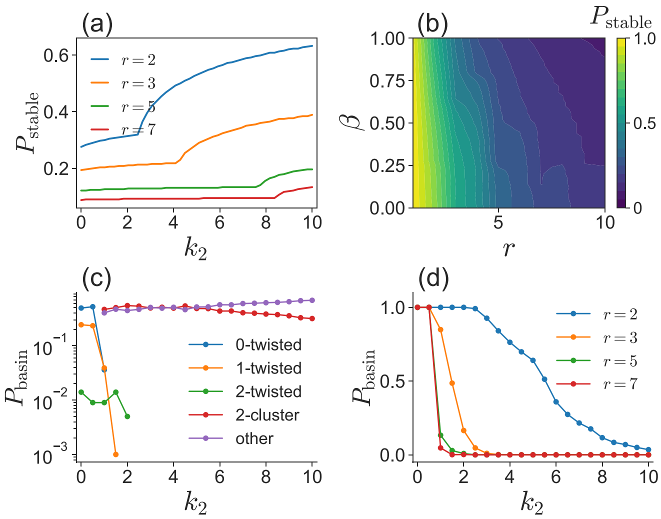


FIG. 9. Stability of twisted states in adaptive networks with different coupling ranges. (a) Fraction of linearly stable twisted states as a function of $k_2$ for different coupling ranges. (b) Distribution of the linear stability ratio in the $(r, \beta)$ parameter space. To ensure smooth curves, the theoretical linear stability analysis was performed with $N = 830$ nodes. (c) Basin size for each state as a function of $k_2$ for the coupling range $r = 5$ and $N = 83$. (d) Basin stability of all twisted states as a function of $k_2$ for different coupling ranges with $N = 83$ nodes. Other parameters are set as (a), (c), and (d) $\alpha = 0$, $\beta = 1$; (b) $k_2 = 10$. An increase in the coupling range weakens both the linear stability and basin stability of twisted states.

is expected to decrease. In other words, the enhancement of the degree of pairwise self-adaptation will relatively enhance the higher-order interactions. In this case, the linear stability of the twisted state may be enhanced and the system is more likely to evolve to a nontwisted state, leading to a weakening of the basin stability of the twisted state instead. Support for this speculation is provided by Fig. 8. Figure 8(a) shows the relationship between the linear stability of the twisted state and the higher-order coupling strength for two different pairs of adaptations ($\alpha = 0.5$ and $\alpha = 1.0$). The results show that the linear stability of the twisted states both increase rapidly from a lower value then stabilize. When $k_2 < 2$, the linear stability of the twisted state with $\alpha = 1.0$ is greater than that with $\alpha = 0.5$. When $k_2 > 2$, the stability of the two states tends to be the same because the higher-order interactions dominate at this point, making the effect of pairwise interactions negligible. Figure 8(b) shows the variation between twisted and nontwisted state basins. It can be seen that the shrinkage of the twisted state basin is significantly faster in the $\alpha = 1.0$ case when $k_2 < 4$. This phenomenon suggests that pairwise adaptation enhances the robustness of the twisted state under local perturbations by modulating the coupling strength, while simultaneously reducing its global attraction ability. Consequently, the system becomes more likely to evolve to the nontwisted state.

### C. Other network structures

In the following, we investigate how varying the coupling range shapes the stability properties of twisted states in adaptive networks. As shown in Fig. 9(a), the fraction of linearly stable twisted states $P_{\mathrm{stable}}$ decreases with increasing coupling range $r$, indicating that larger coupling ranges weaken the linear stability of twisted states. Furthermore, in the two-dimensional parameter space $(r, \beta)$ [Fig. 9(b)], the linear stability consistently decreases as $r$ increases for different values of the adaptive parameter $\beta$. In other words, when the coupling strength is fixed, variations in the adaptive parameter exert only a limited influence on the linear stability of twisted states. Correspondingly, we further investigate the basin sizes of the system with coupling range $r = 5$ for $N = 83$ nodes. By performing $10^4$ simulations with random initial conditions, we obtain the probabilities of the system converging to different states, as shown in Fig. 9(c). The results indicate that the basins of twisted states shrink rapidly as $k_2$ increases. Unlike the case of $r = 2$, where the disappearance of twisted states leaves other states dominant, for $r = 5$ the two-cluster state also becomes a major attractor once the twisted states vanish. Figure 9(d) further illustrates the basin size $P_{\mathrm{basin}}$ of all twisted states as a function of the higher-order coupling strength $k_2$ for $N = 83$ nodes. When the coupling range is small, $P_{\mathrm{basin}}$ decreases gradually with increasing $k_2$; however, for larger coupling ranges, increasing $k_2$ results in a rapid collapse of the basin.

The underlying mechanism is that a larger coupling range brings distant nodes with large phase differences into strong interaction. This "long-range pulling" effect tends to flatten phase differences and drives the system toward more homogeneous or lower-energy states, thereby undermining the constraints needed to sustain twisted gradients. At the level of small perturbations, this effect reduces the ability of twisted states to resist disturbances, as reflected in the decrease of $P_{\mathrm{stable}}$ with larger $r$. In the dynamical evolution from random initial conditions, long-range coupling also facilitates the transition of the system into two-cluster or other nontwisted states, leading to a significant reduction in the basin stability $P_{\mathrm{basin}}$. Therefore, increasing the coupling range reduces the stability of twisted states at both the linear and nonlinear levels.

Finally, we investigate the influence of the higher-order adaptive exponent on the stability of attractors in random hypergraphs. The random hypergraph is constructed with

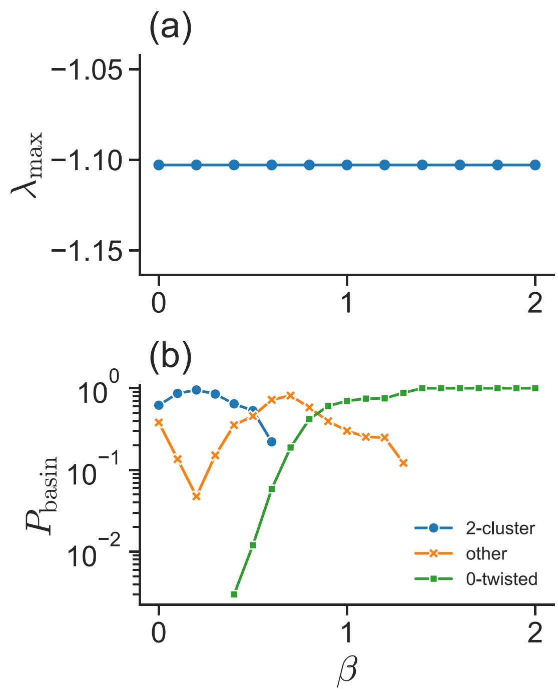


FIG. 10. In random hypergraphs, the higher-order adaptive parameter does not affect the linear stability of synchronization. However, as the higher-order adaptive exponent increases, the basin of synchronization gradually expands. (a) The maximum Lyapunov exponent of the fully synchronized state and (b) the relative basin sizes of synchronization, two-cluster, and other states as functions of the higher-order adaptive exponent. Random hypergraph parameters: $N = 83$, the probabilities of forming hyperedges between two and three nodes are $20/N$ and $20/N^2$, respectively. Other parameters: $\alpha = 0, k_1 = k_2 = 1$.

$N = 83$ nodes, where any pair of nodes and any triplet of nodes are connected with probabilities $20/N$ and $20/N^2$, respectively. The local order parameter of each node is defined as

$$O_i = \frac{\left[\sum_{j=1}^{N} A_{ij} e^{i(\theta_j-\theta_i)} + \frac{1}{2!}\sum_{j=1}^{N}\sum_{k=1}^{N} B_{ijk} e^{i(\theta_j+\theta_k-2\theta_i)}\right]}{\sum_{j=1}^{N} A_{ij} + \frac{1}{2!}\sum_{j=1}^{N}\sum_{k=1}^{N} B_{ijk}}. \quad (12)$$

As shown in Fig. 10(a), the higher-order adaptive exponent $\beta$ has no effect on the linear stability of the fully synchronized state. This is because full synchrony is the only attractor in random hypergraphs, where the local order parameter of every node satisfies $|O_i| = 1$. Hence, the Jacobian matrix of the adaptive system is identical to that of the nonadaptive one, and the maximum Lyapunov exponent remains unchanged. Figure 10(b) presents the statistical results obtained from $10^4$ realizations with random initial conditions. When the higher-order adaptive exponent $\beta$ is small, the system predominantly converges to the two-cluster or other nonsynchronized states. As $\beta$ increases, similar to our previous observations in Fig. 5, the system tends to evolve toward more ordered configurations, and the basin of attraction for full synchrony gradually expands.

## IV. CONCLUSIONS

In this paper we investigate the effect of adaptation on the stability of twisted states in a network of nonlocally coupled oscillators. The adaptation is based on a mechanism where the local order parameter modulates the coupling strength. Unlike the previous discussion, which focused solely on the linear stability of twisted states from a theoretical perspective [49], we further investigate their linear stability through numerical simulations. Specifically, the system is initialized as a twisted state with a small perturbation, and its time evolution is monitored. If the system remains in the original twisted state after sufficiently long evolution, the state is regarded as linearly stable. Numerical and theoretical results show that an increase in the degree of higher-order adaptivity decreases the linear stability of the twisted state. We also analyze the reasons why the theoretical results are smaller than those of the numerical simulations. For twisted states with theoretical $\lambda_{max}$ slightly greater than zero, no significant phase change is observed in the finite-time numerical simulations.

Conversely, an increase in the degree of higher-order adaptivity leads to an expansion of the twisted state's basin of attraction. This expansion facilitates the convergence of more stochastic initial conditions toward the ordered state. We also introduce pairwise adaptation and find that it enhances the linear stability of the twisted state but shrinks its basin. In other network topologies, we found that increasing the coupling range reduces the stability of twisted states. In random hypergraphs, however, the higher-order adaptive exponent has no impact on the linear stability of synchronization, but it significantly expands its basin of attraction.

Higher-order adaptation carries an opposite effect on the response of the nonlocal coupled network under local and global perturbations. The same negative correlation between linear stability and basin stability is observed in systems undergoing successive Hopf bifurcations [14]. Moreover, an increase in the strength of higher-order coupling can expand the basin size in both the embedded and incoherent states [48,50]. Higher-order adaptation makes the ordered states easier to detect and slows the tendency of the system towards entropy increase. This effect is important for increasing the stability of the system.

Finally, the present study provides a distinct perspective on twisted state stability compared with our previous based phase lag work [49]. Here the central mechanism is a state-dependent adaptive feedback governed by the real-valued local order parameter $|O_i|$, rather than a fixed phase shift in the interaction term. Although this adaptive rule is introduced in a minimal form, it has a transparent physical meaning, since $|O_i|$ quantifies the coherence of the local neighborhood and therefore acts as a natural feedback signal for regulating the effective coupling strength. In this way, the model offers an effective description of activity-dependent local interactions. Under this framework, pairwise and higher-order adaptation lead to qualitatively different behaviors in both linear stability and basin stability. In addition, by combining analytical derivations with direct numerical simulations of perturbed twisted states, the present work goes beyond purely theoretical linear-stability analysis and provides explicit dynamical verification of the predicted stability properties. These results extend the study of twisted state stability to adaptive networks and deepen the understanding of how local feedback regulation influences the emergence and robustness of ordered collective states.

## ACKNOWLEDGMENTS

This work is supported by National Natural Science Foundation of China under Grant No. 12175080, and self-determined research funds of CCNU from the colleges' basic research and operation of MOE under Grant No. CCNU25JC012.

## DATA AVAILABILITY

The data and code supporting the findings of this article are openly available [51].

[1] D. Witthaut, F. Hellmann, J. Kurths, S. Kettemann, H. Meyer-Ortmanns, and M. Timme, Collective nonlinear dynamics and self-organization in decentralized power grids, Rev. Mod. Phys. **94**, 015005 (2022).

[2] P. Schultz, J. Heitzig, and J. Kurths, Detours around basin stability in power networks, New J. Phys. **16**, 125001 (2014).

[3] S. Arik, An analysis of global asymptotic stability of delayed cellular neural networks, IEEE Trans. Neural Networks **13**, 1239 (2002).

[4] Z. Wang, Y. Liu, and X. Liu, On global asymptotic stability of neural networks with discrete and distributed delays, Phys. Lett. A **345**, 299 (2005).

[5] C. Giusti, R. Ghrist, and D. S. Bassett, Two's company, three (or more) is a simplex, J. Comput. Neurosci. **41**, 1 (2016).

[6] D. Pattanayak, A. Mishra, S. K. Dana, and N. Bairagi, Bistability in a tri-trophic food chain model: Basin stability perspective, Chaos **31**, 073124 (2021).

[7] T. Gross, L. Rudolf, S. A. Levin, and U. Dieckmann, Generalized models reveal stabilizing factors in food webs, Science **325**, 747 (2009).

[8] Y. Zhang, V. Latora, and A. E. Motter, Unified treatment of synchronization patterns in generalized networks with higher-order, multilayer, and temporal interactions, Commun. Phys. **4**, 195 (2021).

[9] M. Lucas, G. Cencetti, and F. Battiston, Multiorder Laplacian for synchronization in higher-order networks, Phys. Rev. Res. **2**, 033410 (2020).

[10] S. Leng, W. Lin, and J. Kurths, Basin stability in delayed dynamics, Sci. Rep. **6**, 21449 (2016).

[11] N. Xu, D. Frenkel, and A. J. Liu, Direct determination of the size of basins of attraction of jammed solids, Phys. Rev. Lett. **106**, 245502 (2011).

[12] Y. Zhang, Z. G. Nicolaou, J. D. Hart, R. Roy, and A. E. Motter, Critical switching in globally attractive chimeras, Phys. Rev. X **10**, 011044 (2020).

[13] P. J. Menck, J. Heitzig, N. Marwan, and J. Kurths, How basin stability complements the linear-stability paradigm, Nat. Phys. **9**, 89 (2013).

[14] P. C. Böttcher, B. Schäfer, S. Kettemann, C. Agert, and D. Witthaut, Local versus global stability in dynamical systems with consecutive Hopf bifurcations, Phys. Rev. Res. **5**, 033139 (2023).

[15] F. Malizia, S. Lamata-Otín, M. Frasca, V. Latora, and J. Gómez-Gardeñes, Hyperedge overlap drives explosive transitions in systems with higher-order interactions, Nat. Commun. **16**, 555 (2025).

[16] F. Battiston, G. Cencetti, I. Iacopini, V. Latora, M. Lucas, A. Patania, J.-G. Young, and G. Petri, Networks beyond pairwise interactions: Structure and dynamics, Phys. Rep. **874**, 1 (2020).

[17] X. Ji and X. Li, Chimera-inspired dynamics: When higher-order interactions are expressed differently, Phys. Rev. E **110**, 044204 (2024).

[18] Y. Zhang, M. Lucas, and F. Battiston, Higher-order interactions shape collective dynamics differently in hypergraphs and simplicial complexes, Nat. Commun. **14**, 1605 (2023).

[19] I. Iacopini, G. Petri, A. Barrat, and V. Latora, Simplicial models of social contagion, Nat. Commun. **10**, 2485 (2019).

[20] G. F. de Arruda, M. Tizzani, and Y. Moreno, Phase transitions and stability of dynamical processes on hypergraphs, Commun. Phys. **4**, 24 (2021).

[21] A. Santoro, F. Battiston, G. Petri, and E. Amico, Higher-order organization of multivariate time series, Nat. Phys. **19**, 221 (2023).

[22] J. Faskowitz, R. F. Betzel, and O. Sporns, Edges in brain networks: Contributions to models of structure and function, Netw. Neurosci. **6**, 1 (2022).

[23] A. P. Millán, J. J. Torres, and G. Bianconi, Explosive higher-order Kuramoto dynamics on simplicial complexes, Phys. Rev. Lett. **124**, 218301 (2020).

[24] T. Carletti, L. Giambagli, and G. Bianconi, Global topological synchronization on simplicial and cell complexes, Phys. Rev. Lett. **130**, 187401 (2023).

[25] P. S. Skardal and A. Arenas, Higher order interactions in complex networks of phase oscillators promote abrupt synchronization switching, Commun. Phys. **3**, 218 (2020).

[26] S. Dutta, A. Mondal, P. Kundu, P. Khanra, P. Pal, and C. Hens, Impact of phase lag on synchronization in frustrated Kuramoto model with higher-order interactions, Phys. Rev. E **108**, 034208 (2023).

[27] M. H. Matheny *et al.*, Exotic states in a simple network of nanoelectromechanical oscillators, Science **363**, eaav7932 (2019).

[28] G. S. Medvedev and X. Tang, Stability of twisted states in the Kuramoto model on Cayley and random graphs, J. Nonlinear Sci. **25**, 1169 (2015).

[29] A. Díaz-Guilera, D. Marinelli, and C. J. Pérez-Vicente, Exploring the interplay of excitatory and inhibitory interactions in the Kuramoto model on circle topologies, Chaos **34**, 043134 (2024).

[30] A. Townsend, M. Stillman, and S. H. Strogatz, Dense networks that do not synchronize and sparse ones that do, Chaos **30**, 083142 (2020).

[31] D. Yu, Y. Wu, Q. Ding, T. Li, and Y. Jia, Emergence of phase clusters and coexisting states reveals the structure-function relationship, Phys. Rev. E **109**, 054312 (2024).

[32] X. Wang, D. Yu, T. Li, X. Li, W. Huang, X. Zhan, and Y. Jia, Effects of spike-time-dependent plasticity on stochastic resonance in excitatory-inhibitory neuronal networks, Nonlinear Dyn. **112**, 12435 (2024).

[33] M. Ogura and V. M. Preciado, Epidemic processes over adaptive state-dependent networks, Phys. Rev. E **93**, 062316 (2016).

[34] T. Gross, C. J. D. D' Lima, and B. Blasius, Epidemic dynamics on an adaptive network, Phys. Rev. Lett. **96**, 208701 (2006).

[35] T. Gross and B. Blasius, Adaptive coevolutionary networks: A review, J. R. Soc. Interface **5**, 259 (2008).

[36] L. F. Abbott and S. B. Nelson, Synaptic plasticity: Taming the beast, Nat. Neurosci. **3**, 1178 (2000).

[37] E. L. Lameu, F. S. Borges, K. C. Iarosz, P. R. Protachevicz, C. G. Antonopoulos, E. E. N. Macau, and A. M. Batista, Short-term and spike-timing-dependent plasticity facilitate the formation of modular neural networks, Commun. Nonlinear Sci. Numer. Simul. **96**, 105689 (2021).

[38] V. Marceau, P.-A. Noël, L. Hébert-Dufresne, A. Allard, and L. J. Dubé, Adaptive networks: Coevolution of disease and topology, Phys. Rev. E **82**, 036116 (2010).

[39] D. Yu, X. Li, X. Wang, W. Huang, X. Hu, and Y. Jia, Community modularity structure promotes the evolution of phase clusters and chimeralike states, Phys. Rev. E **111**, 034311 (2025).

[40] M. S. Anwar, S. N. Jenifer, P. Muruganandam, D. Ghosh, and T. Carletti, Synchronization in adaptive higher-order networks, Phys. Rev. E **110**, 064305 (2024).

[41] S. N. Jenifer, D. Ghosh, and P. Muruganandam, Synchronization transitions in adaptive simplicial complexes with cooperative and competitive dynamics, Chaos **34**, 123155 (2024).

[42] P. Rajwani, A. Suman, and S. Jalan, Tiered synchronization in Kuramoto oscillators with adaptive higher-order interactions, Chaos **33**, 061102 (2023).

[43] R. Ghosh, M. S. Anwar, D. Ghosh, J. Kurths, and M. D. Shrimali, Transitions to synchronization in adaptive multilayer networks with higher-order interactions, Phys. Rev. E **111**, 064219 (2025).

[44] M. Manoranjani, V. R. Saiprasad, R. Gopal, D. V. Senthilkumar, and V. K. Chandrasekar, Phase transitions in an adaptive network with the global order parameter adaptation, Phys. Rev. E **108**, 044307 (2023).

[45] D. Biswas and S. Gupta, Effect of adaptation functions and multilayer topology on synchronization, Phys. Rev. E **109**, 024221 (2024).

[46] D. A. Wiley, S. H. Strogatz, and M. Girvan, The size of the sync basin, Chaos **16**, 015103 (2006).

[47] B. Li and N. Uchida, Effect of mobility on collective phase dynamics of nonlocally coupled oscillators with a phase lag, Phys. Rev. E **106**, 054210 (2022).

[48] Y. Zhang, P. S. Skardal, F. Battiston, G. Petri, and M. Lucas, Deeper but smaller: Higher-order interactions increase linear stability but shrink basins, Sci. Adv. **10**, eado8049 (2024).

[49] X. Wang, D. Yu, T. Li, X. Li, Y. Xie, and Y. Jia, Stability of twisted states: The role of phase lag, pairwise and higher-order interactions, Phys. Rev. E **112**, 024202 (2025).

[50] S. Kundu and D. Ghosh, Higher-order interactions promote chimera states, Phys. Rev. E **105**, L042202 (2022).

[51] Local-order-parameter-adaptation, GitHub, 2026, https://github.com/XueqinWangya/Local-Order-Parameter-Adaptation.git.